energies

MDPI

Article

Ultimate Limit State Scour Risk Assessment of a Pentapod Suction Bucket Support Structure for Offshore Wind Turbine

Young-Jin Kim [1], Duc-Vu Ngo [1], Jang-Ho Lee [2] and Dong-Hyawn Kim [3,*]

[1] Department of Ocean Science and Engineering, Kunsan National University, Gunsan 54150, Korea; ioi1937@nate.com (Y.-J.K.); ngoducvubk@gmail.com (D.-V.N.)
[2] School of Mechanical Convergence System Engineering, Kunsan National University, Gunsan 54150, Korea; jhlee@kunsan.ac.kr
[3] School of Architecture and Coastal Construction Engineering, Kunsan National University, Gunsan 54150, Korea
* Correspondence: eastlite@kunsan.ac.kr

Abstract: Scour risk assessment considering reaction force at foundation was proposed and applied to newly developed pentapod suction bucket support structures for a 5.5 MW offshore wind turbine under ultimate limit state environmental load. Scour hazard was obtained according to scour depth by using an empirical formula, which is the function of marine environmental conditions such as significant wave height, significant period, and current velocity. Fragility of the pentapod support structure was evaluated using the bearing capacity limit state criterion under ultimate limit state load case. Scour risk was assessed by combining the scour hazard and the fragility. Finally, scour risk of the developed pentapod suction bucket support structure under ultimate limit state has been assessed.

Keywords: offshore wind turbine; suction bucket; pentapod suction bucket; scour; scouring fragility; scour risk

check for updates

Citation: Kim, Y.-J.; Ngo, D.-V.; Lee, J.-H.; Kim, D.-H. Ultimate Limit State Scour Risk Assessment of a Pentapod Suction Bucket Support Structure for Offshore Wind Turbine. *Energies* **2022**, *15*, 2056. https://doi.org/10.3390/en15062056

Academic Editor: Paweł Lizęga

Received: 23 January 2022
Accepted: 7 March 2022
Published: 11 March 2022

1. Introduction

Suction Bucket (SB) is a highly competitive foundation solution among the several types of foundations currently implemented to support offshore wind turbines (OWT) due to their quick and noise-free installation. They are also a more economical solution compared to other foundations, especially for a large-scale wind farm [1]. The main design factors of such a SB support structure are the horizontal bearing capacity and the stiffness of the foundation. Latini and Zania, 2017 [2] investigated the dynamic behavior of SB and concluded that the skirt length of a SB is an important parameter that determines the dynamic behavior, and the horizontal bearing capacity is greatly affected by the ratio of the bucket diameter and length. Foundation stiffness is strongly dependent on the relative density of sand and the bucket's geometry and has been investigated in a series of studies [3–5]. When existing SB support structures are installed in area where the geological structure is a shallow soft-layer soil on top of a hard-layer soil, there is a problem that the SB diameter must be abnormally large to fulfill the required bearing capacity. To solve this problem, a pentapod suction bucket (PSB) support structure was developed by Ngo et al. [6], and a seismic fragility analysis was performed on the developed support structure.

Scouring is recognized as a risk factor that weakens the bearing capacity around the turbine support structures. Accordingly, local scour around OWT foundations has been studied by many researchers [7–9], and most studies have used scale model tests and numerical simulations. A series of laboratory experiments were conducted by Hu et al. [10] to investigate the scour development around tripod foundation in combined waves and the current. The influence of installation angles, KC number, and the ratio of velocities U_{cw} on the scour depth were also examined. In another study, Hu and his colleagues proposed a method to predict the equilibrium scour depth around the umbrella suction anchor foundation [11]. In order to reduce the risk of scouring, a prevention method is installed around the support structures [12]. Since the scouring protection method incurs costs, a reasonable risk assessment by scouring is necessary for the development of an economical power generation complex. Studies on the behavior of supporting structures by scouring have not been actively performed. A few studies have been recently reported. Yi et al., 2013 studied the effect of scour on dynamic instability of monopile offshore wind turbines [13]. In the study, the natural frequency change according to seabed scour depth (SD) was analyzed and possible resonance due to scour was discussed. Ma et al., 2018 [14] studied the effect of local scour around foundation on the dynamic behavior of the support structure. Both studies revealed that scour had little effect on frequencies but had some effect on dynamic behavior. Scour risk assessment around marine structures has also been performed in many studies. Yanmaz and Salamak [15] evaluated the risk of the scouring process at bridge piers. They established a probabilistic model for the scour depth predictions through empirical equations in the dimensional state. Khalid et al. [16] applied a non-linear regression-based technique to calculate the reliability of scour depth values at bridge piers installed in cohesive bed sediments. A study that evaluated a reliability-based probabilistic of the wave-induced scour depth around marine structure piles was performed by Homaei et al. [17]; they developed a probabilistic model by using an artificial intelligence method so as to predict the scour depth at pile groups under regular waves. However, these studies were conducted on monopiles, and the risk of scouring could not be evaluated quantitatively. Kim et al., 2020, proposed a scouring risk assessment method by combining the scouring hazard and fragility of the support structure [18]. They showed, for the first time, that scour risk can be evaluated by modifying the seismic risk assessment approach. Scour fragility of a tripod suction bucket (TSB) was found by defining a critical displacement at foundation. Ngo et al. recently reported a seismic fragility analysis of PSB support structure and showed that the seismic performance of the pentapod is superior to that of the TSB [6].

In this study, a scour risk analysis was performed to evaluate the stability of the newly developed PSB support structure at an ultimate limit state. For this, the hazard according to the scour depth was calculated. For the scour depth, an empirical formula defined as a function of marine environmental variables was used. As for the fragility, the bearing capacity limit state according to the ultimate load was used instead of the fragility function based on displacement [18]. The safety factor (SF) was applied to the reaction force of the PSB to determine how the scour risk was affected.

In the second chapter, theoretical background of scour risk assessment is explained. How to calculate scour hazard, fragility and risk are shown in detail. In the third chapter, why a PSB is developed and features of PSB are explained. After that, numerical analysis and conclusions are described in turn.

2. Scour Risk

2.1. Probability of SD

During the design process, the capacity of OWT substructure (SB foundation in this study) is designed against external loads such as wind, wave, and so on. The magnitude of these external loads is governed by wind speed, wave height or current velocity, etc. and their effects have also been verified through various design load cases (DLCs). Nevertheless, the initial OWT foundation's design capacity may be decreased due to several reasons, with local scouring around its foundation being the most common. In previous studies, maximum equilibrium SD was suggested as a keyword to evaluate the influence of scouring on the structure. This leads to unnecessary costs in the design and operation of an OWT, especially when the scale of the wind farm project is large. Therefore, it is necessary to consider scouring as a probabilistic parameter in risk analysis.

In this study, the empirical formula of Equation (1) proposed by Sumer and Fredsoe, 2001 [19] is used to obtain the probability distribution of SD. In Equation (1), the SD is a function of the Keulegan–Carpenter (KC) number and the parameter U_{cw}, in which KC was defined by the peak spectrum period (T_p), pile diameter (D), and maximum value of the undisturbed orbital velocity at the sea bottom just above the wave boundary layer (U_m).

$$\frac{S}{D} = \frac{S_C}{D}[1 - \exp\{-A(KC - B)\}],\ KC \geq 4 \tag{1}$$

where: S: SD; S_C: SD in the case of steady current alone; D: pile diameter; $KC = U_m T_p/D = 2\pi a/D$; $A = 0.03 + 0.75U_{cw}^{2.6}$; $B = 6\exp(-4.7U_{cw})$; $U_{cw} = U_c/(U_c + U_m)$; U_C: the undisturbed current velocity at the distance, y = D/2 from the bed; U_m: maximum value of the undisturbed orbital velocity at the bed; T_p: peak spectrum period; a: the amplitude of the motion of water particles at the bed.

In Equation (1), the SD probability distribution can be obtained by considering the variability of KC parameter. The variability of KC is governed by the variability of height and period of the significant wave. The probability density function (PDF) of SD obtained here is a scour hazard for risk analysis and denoted by $f_{SD}(x)$.

2.2. Scour Fragility

The fragility curve of structures under earthquakes has been proposed by Shinozuka et al., 2000 [20]. These fragility curves are represented by logarithmic normal distribution functions, and the two coefficients of the lognormal distribution function, median and logarithmic standard deviation, are obtained by the maximum likelihood estimation method. For the *k*-th damage among various damage stages, the fragility curve can be expressed as:

$$F_k(x) = \Phi\left|\frac{\ln\left(\frac{x}{c_k}\right)}{\zeta_k}\right| \tag{2}$$

where Φ is the standard normal cumulative distribution function, c_k is the median, and ζ_k is the logarithmic standard deviation.

When assessing structural fragility, a limit state should be determined first. There are various limit states such as serviceability limit state (SLS), fatigue limit state (FLS) and ultimate limit states (ULS). Kim et al. found fragility curves of TSB based on displacement [10]. Because the displacement of the bucket causes a serviceability problem rather than the destruction of the support structure, it is a fragility based on SLS. However, the purpose of this study is to evaluate bearing capacity of a newly designed PSB under ultimate load case. Therefore, an event in which the reaction force of the bucket exceeds the allowable bearing capacity was defined as the failure. Therefore, the fragility of this study can be called ULS based.

2.3. Scour Risk

By combining the probability of SD (hazard) and the scour fragility curve of the structure, the scour risk can be calculated as in Equation (3).

$$P_f = \int_{x_0}^{x_{max}} f_{SD}(x) F_k(x) dx \tag{3}$$

where x_{max} and x_0 is the maximum possible SD and the lowest SD, respectively.

3. Development of PSB Support Structure

3.1. Background

A ground survey was carried out on the coast of Gunsan, Southwest of Korea, prior to the design and installation of a 5.5 MW OWT. Figure 1a is the expected installation location, while Figure 1b and Table 1 show the ground investigation results. It is observed in Figure 1b that a bedrock layer appears at a depth of 7.5 m, and when an offshore wind turbine supported by suction bucket foundation is installed here, the length of the suction bucket skirt must be less than 7.5 m. Since the skirt length is limited, it is necessary to increase the bucket diameter to reinforce the overturning resistance and improve bearing capacity. However, various problems include the lack of manufacturing facilities for large-diameter suction buckets, transportation and installation equipment, etc. Moreover, increasing the diameter can make the spacing between the buckets too narrow, leading to overlap stress. Hence, developing a multi-pod suction bucket support structure that exhibits equivalent support is necessary.

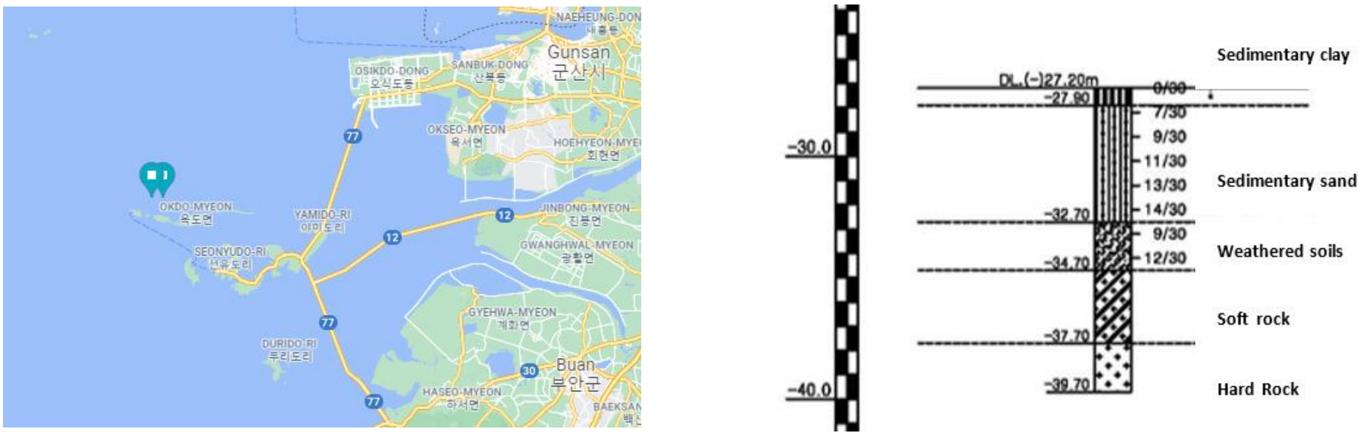

(**a**) (**b**)

Figure 1. Installation area: (**a**) map; (**b**) soil layer.

Table 1. Soil profile of survey site.

Soil Layer	Depth (m)	Unit Weight (kN/m^3)	Elasticity (MPa)	Internal Friction Angle (deg)	Cohesion Yield Stress (kPa)	Poisson's Ratio
Upper clay	0.0~0.7	17	25.00	32.3	-	0.491
Upper sand	0.7~4.8	17.5	35.56	32.3	5	0.400
Lower sand	4.8~7.5	17.5	67.48	37.0	5	0.400
Weathered rock	7.5~	20.0	76.00	32.0	-	0.450

3.2. Development of PSB Support Structure

Figure 2 shows the top view and thrust direction of the PSB model. The spacing (R) between each bucket and the center of the tower is assumed to be the same. According to the thrust direction, as shown in Figure 2, the pull-out resistance (V_t) and compression resistance (V_c) are indicated by red and blue dots, respectively. Then, the resistance moment (M_R) can be calculated as in Equations (4)–(7).

$$M_R = V_t b_1 + 2V_t b_2 \tag{4}$$

$$b_1 = R + R\cos(36^\circ) = 1.809R \tag{5}$$

$$b_2 = R\cos(36^\circ) + R\cos(72^\circ) = 1.118R \tag{6}$$

$$M_R = 1.809V_tR + 2.236V_tR = 4.045V_tR \tag{7}$$

When the number of buckets is 3 to 6, the moment of resistance (M_R) can be calculated the same way, and the corresponding normalized resistance moments are shown in Figure 3 [6].

It can be seen from Figure 3 that the PSB has better pull-out and compression resistance than other multi-pod support structures. Therefore, a PSB support structure using five buckets was finally developed. Figure 4 shows the developed PSB support structure.

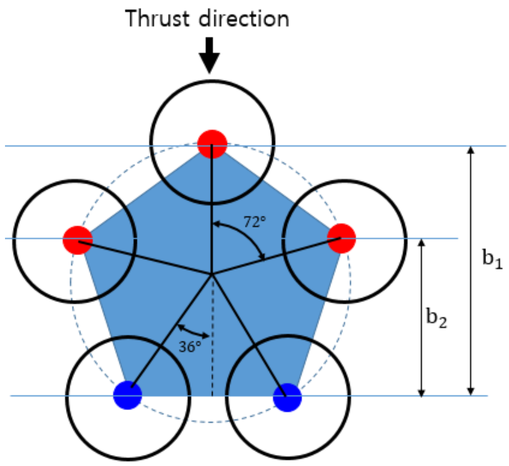

Figure 2. Top view of PSB [6].

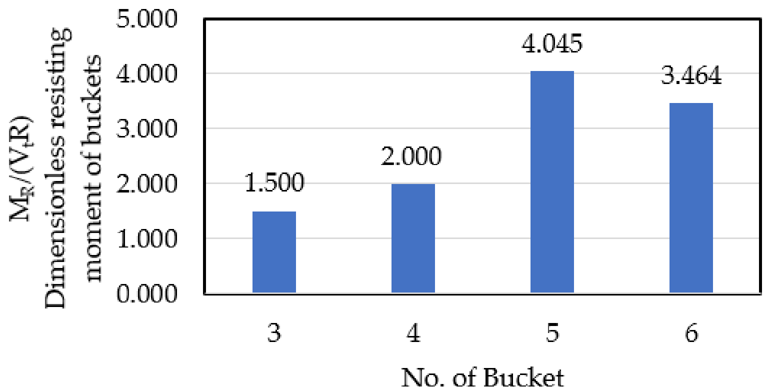

Figure 3. Dimensionless resisting moment of buckets.

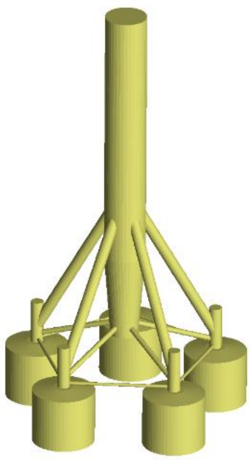

Figure 4. Pentapod support structure.

4. Numerical Example

4.1. Wind Turbine and Support Structure Model

Figure 5 is a 5.5 MW OWT with PSB support structure modeled by Bladed [21]. The hub is located at the height of 110 from sea level and the water depth is 27.723 m. The total height of the offshore wind turbine is 137.723 m. Substructure is a pentapod with five single suction buckets. The geometric and material properties of the supporting tower structure are referred from a previous study [6]. The mechanical characteristics of the seabed connected to a substructure is represented by a soil stiffness matrix.

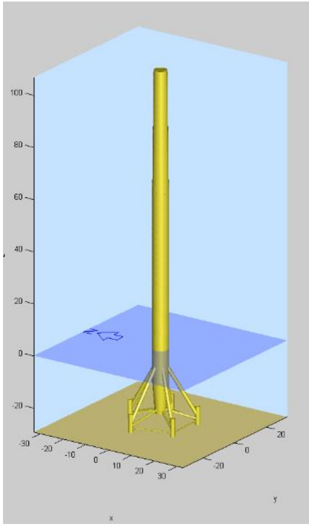

Figure 5. Analysis target.

4.2. Soil-Structure-Interaction Simulation

In order to express the interaction behavior of the suction bucket and the contact ground, a three-dimensional displacement analysis of the bucket-ground model caused by an external force was performed. Then, a stiffness matrix from the analysis was applied to Bladed. The commercially available Finite Element (FE) software ABAQUS [22] was used. The finite element model was shown in Figure 6, the soil was modeled with C3D8R elements, and the bucket foundation modeled by shell element with a diameter (D) of 9 m and a skirt length (L) of 7 m. The center of the bucket top was set as the reference point to apply an external load. Displacements were obtained after sequentially applying external loads in the direction of 6 degrees of freedom (*Fx, Fy, Fz, Mx, My, Mz*) to the reference point. In order to consider the effect of ground nonlinearity, the load in each direction was divided into 10 steps and applied gradually. From the load-response relationship the following equation can be written

$$[\mathrm{d}] = [F][p] \tag{8}$$

where $[\mathrm{d}] = \begin{bmatrix} \Delta_x & \Delta_y & \Delta_z & \theta_x & \theta_y & \theta_z \end{bmatrix}^{\mathrm{T}}$ is the displacement vector; $[p] = [F_x \quad F_y \quad F_z \quad M_x \quad M_y \quad M_z]^{\mathrm{T}}$ the load vector; $[F]$ the flexibility matrix from numerical analysis [23]. Then, the stiffness matrix for ground can be derived as

$$[p] = [K][\mathrm{d}] \tag{9}$$

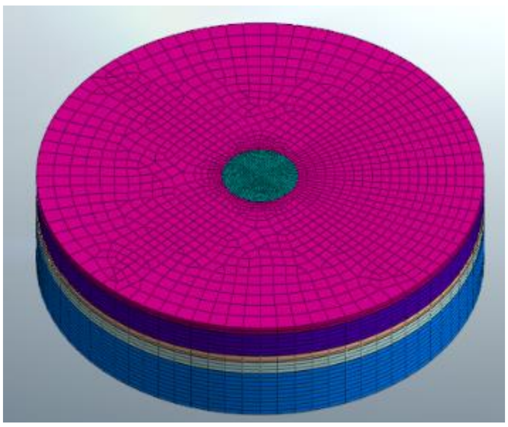

Figure 6. Stiffness matrix analysis model.

The stiffness matrix $[K]$ is the inverse of $[F]$ and obtained in this study for Bladed input as in Figure 7.

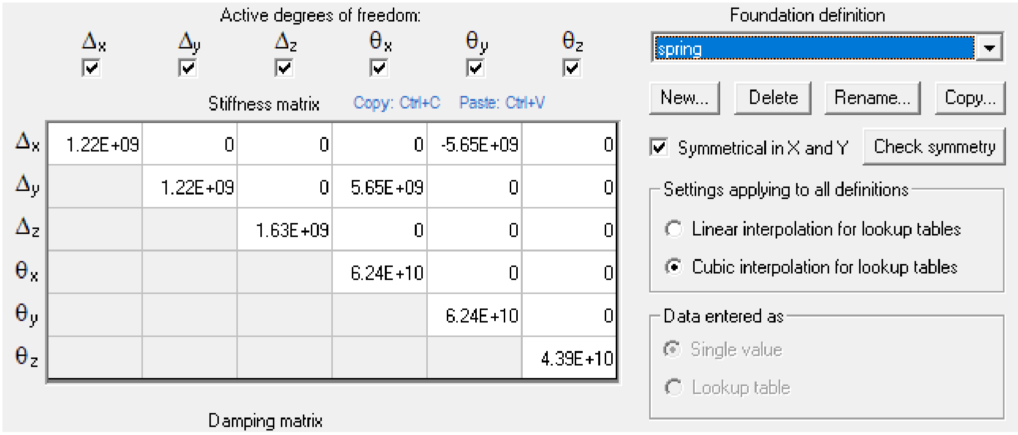

Figure 7. Bladed input for stiffness of foundation spring.

4.3. Wind Thrust

Thrust force by wind is automatically calculated in Bladed. At first, a wind field was generated using the Kaimal model, and a total of 30 cases of thrust force set was calculated by changing the phase of the wind field. Figure 8 shows a time history of thrust force for 10 min calculated by Bladed.

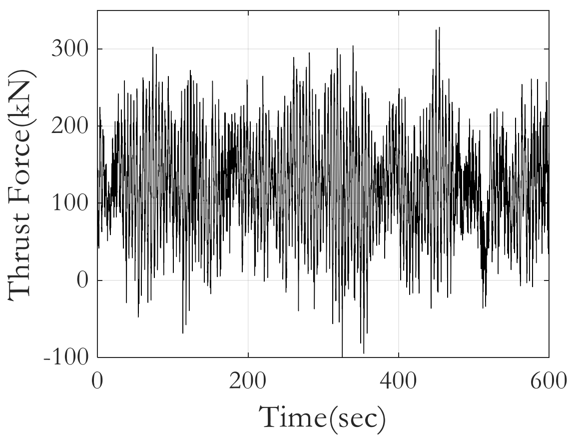

Figure 8. Time history of thrust force.

4.4. Calculation of Wave Load

The Morrison Equation [24] was used to calculate the wave loading acting on the structure in Bladed. To evaluate the risk due to scouring, the most hazardous event caused by the environment during the life cycle was considered. Significant wave height (H_s) and wave period (T_s) are adopted from the HYPA model of the Korea Oceanic Research and Development Institute [25] from 1979 to 2003. Figure 9 shows the probability density function estimated using the Weibull distribution and it can be expressed as Equation (10) where a and b are 5.56 and 9.66, which mean scale and shape parameters, respectively. To obtain the ultimate limit state (ULS) wave load, the significant wave height corresponding to a 50-year return period, H_{s50}, was estimated to be 6.64 m from the PDF. It is the wave height at which an excess probability is 1/50. The significant period was estimated to be 12.9 s using Equation (11) [26].

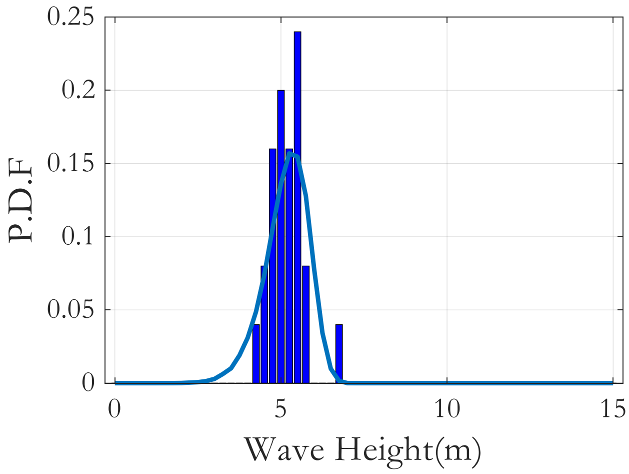

Figure 9. PDF of annual maximum H_s.

$$f_X(x) = \frac{b}{a}\left(\frac{x}{a}\right)^{b-1} e^{-\left(\frac{x}{a}\right)^b} \tag{10}$$

$$T_s = 3.3H_s^{0.63} \tag{11}$$

To simulate the wave acting on the OWT substructure, Bretschneider's wave spectrum with significant wave height (H_s), period (T_s) and frequency (f) is adopted to generate the sea surface elevation time history, it was defined as

$$S(f) = 0.257H_s^2 T_s^{-4} f^{-5} exp\left[-1.03(T_s f)^{-4}\right] \tag{12}$$

Using the Bretschneider spectrum mentioned above, the surface wave elevation profile can be obtained and was shown as Figure 10.

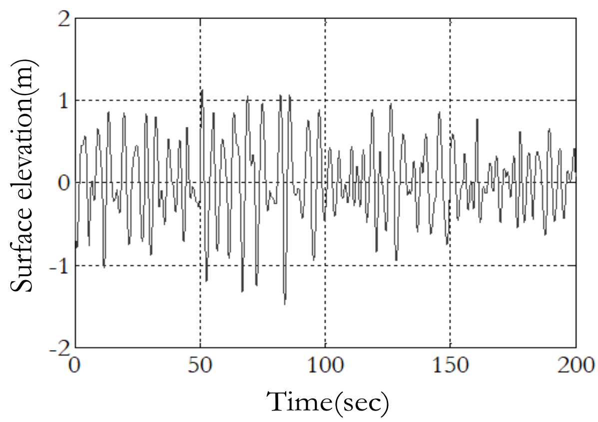

Figure 10. Surface wave elevation.

4.5. Probability Distribution of SD

The probability distribution of SD can be obtained by giving random variability to the variable in Equation (1). The most important among them is the distribution of KC. From the Weibull distribution of Equation (10), the annual maximum significant wave, H_s, is generated and T_s is estimated from Equation (11). Then, peak period T_p corresponding to the H_s and T_s is calculated from the spectrum of Equation (12). Once T_p is calculated scour depth S can be obtained using Equation (1). With 50,000 times random sampling for H_s, KC distribution was developed as Figure 11.

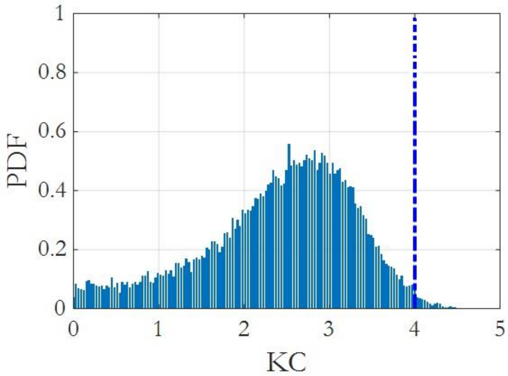

Figure 11. Probability distribution of KC.

The distribution of current speed was collected from the National Oceanic and Atmospheric Research Institute [27]. The estimated distribution of current speed fits the normal distribution, and the mean and standard deviation are 1.34 and 0.19, respectively.

Since only values of KC greater than 4.0 are effective for scour generation, the depth of scour was calculated using the distribution of KC greater than 4.0 and the tidal flow distribution. As a result, the distribution of scour depth was obtained as shown in Figure 12. It was found that a log normal distribution fit well, as shown in Figure 12. Two parameters λ and ζ were 0.75 and 0.55, respectively.

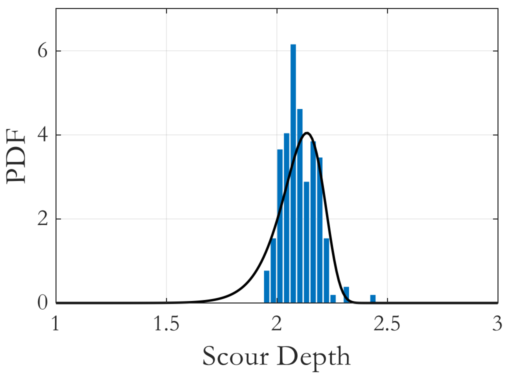

Figure 12. Probability distribution of SD.

4.6. Scouring Fragility Curve

To obtain the fragility curve, the limit state function of PSB is defined as the following equation.

$$g(X) = R_a(SD) - R_{max} \tag{13}$$

where R_a is the allowable bearing capacity of a bucket; R_{max} the maximum reaction force at each bucket. The R_a is a function of scour depth SD since the contact area of a bucket with ground is dependent on SD.

The bearing capacity of a bucket can be calculated numerically in horizontal and vertical directions [28]. For the analysis, the suite of 30 cases were analyzed by changing the seed of the wind field. Based on the structural responses at the mudline location for each case (i.e., reaction force to tension, compression, and horizontal force), the scour fragility was obtained. Accordingly, the maximum reaction members at the mudline obtained by performing a dynamic analysis in the non-sour state were compared with the allowable bearing capacity by SD to determine to what extent SD is safe.

Figure 13a shows the allowable pull-out force of a bucket for each SD. From the figure, the allowable pull-out force rapidly decreases according to SD increase. The tension-bearing capacity of the SB is mainly provided by vertical friction between bucket wall and soil. Therefore, scour reduces bearing capacity in tension direction. Figure 13b compares the allowable tension force at SD of 6.5 m, with the maximum pull out load corresponding to seed variation in wind field. The maximum pull out loads are smaller than the allowable tension capacity. Therefore, no failure is expected in tensional bearing capacity. Figure 14 shows the same results for compressive mode. While Figure 14a shows the allowable compressive force for each SD, Figure 14b compares the maximum compressive force calculated from the structural analysis results and the allowable compressive force at SD of 6.5 m. Both Figures 13 and 14 show that the tension and the compressive forces do not exceed the allowance one because the structural responses are far smaller than the allowable tension and compressive forces in all cases. Therefore, the fragility assessment of support structure in terms of tension and compression force here is not necessary.

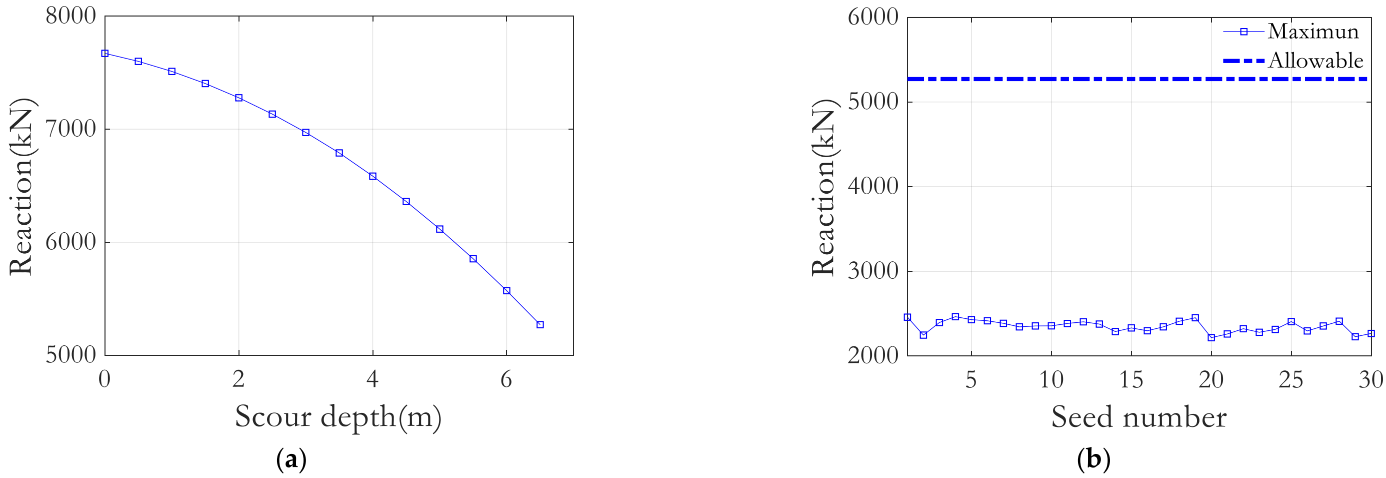

Figure 13. Variation of pull-out reaction: (**a**) allowable reaction; (**b**) reaction at SD = 6.5 cm.

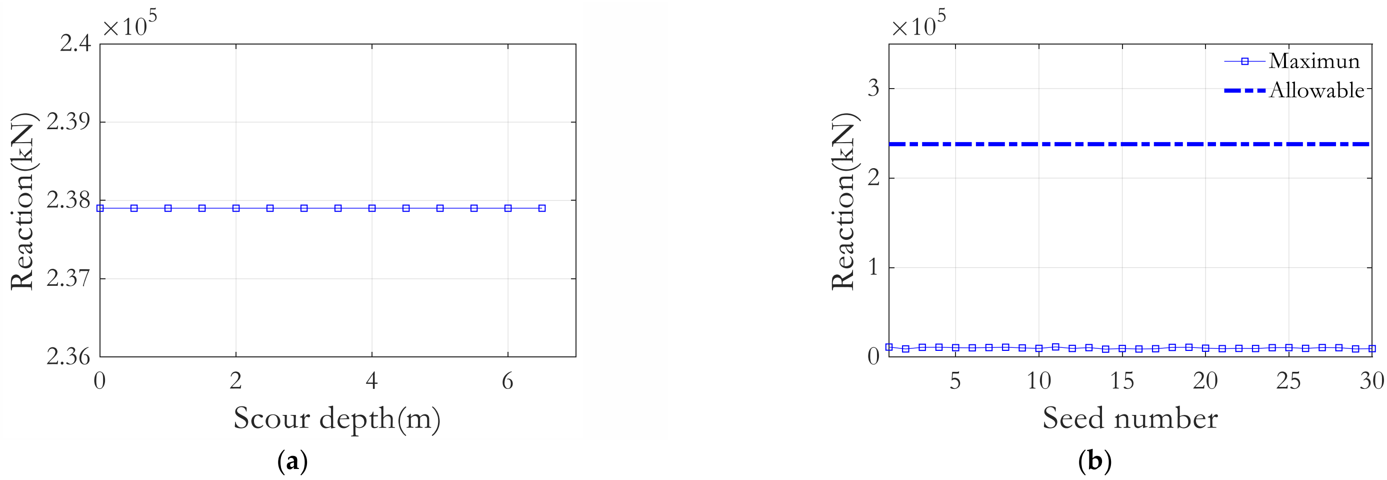

Figure 14. Variation of compressive reaction: (**a**) allowable reaction; (**b**) reaction at SD = 6.5 cm.

The results of horizontal force analysis are given in Figure 15. As shown in Figure 15a, the horizontal bearing capacity decreased as the SD increased. Figure 15b shows the result of comparing the maximum horizontal reaction force and the allowable horizontal force at SD of 4 m. It can be seen from Figure 15b that most of the horizontal reaction force exceeded the allowable horizontal force at the SD of 4.0 m. If more than 4.0 m scour occurs, the probability of failure will increase.

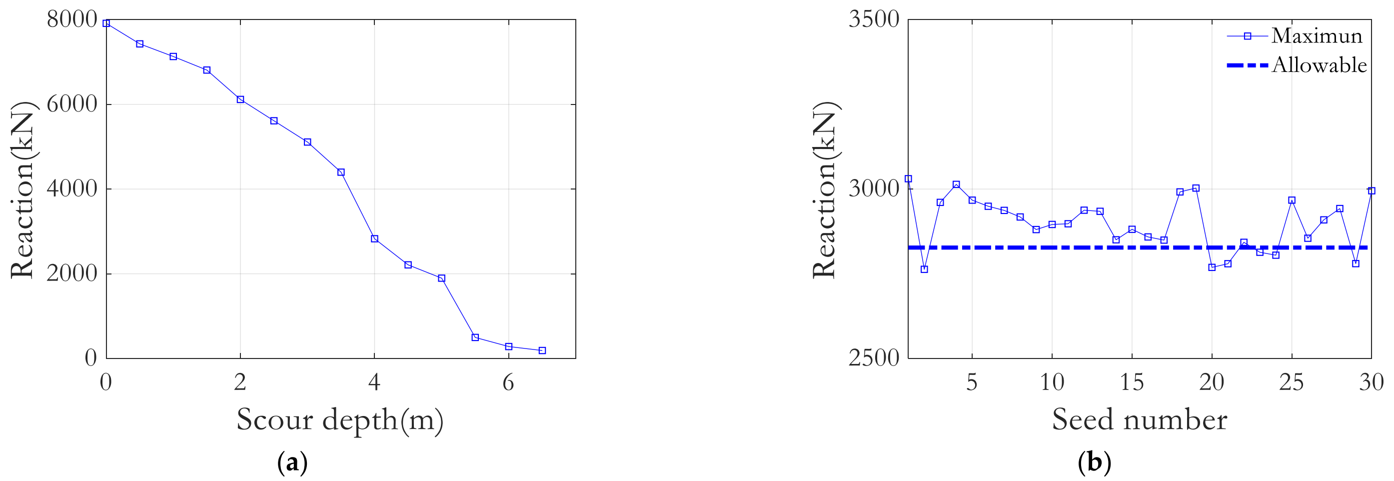

Figure 15. Variation of horizontal reaction: (**a**) allowable reaction; (**b**) reaction at at SD = 4 m.

To see how the safety margin affects the fragility, five cases of safety factors (SFs) were applied to the maximum horizontal reaction force. The fragility curves of the five safety factor cases are shown in Figure 16. The corresponding median and standard deviation values of the fragility curves are listed in Table 2. As can be seen from Figure 16 and Table 2, when the safety factor was not considered, the fragility was more than 50% at SD of around 3.93 m, and when the safety factor 2.0 was considered, the fragility was more than 50% at SD of approximately 2.43 m.

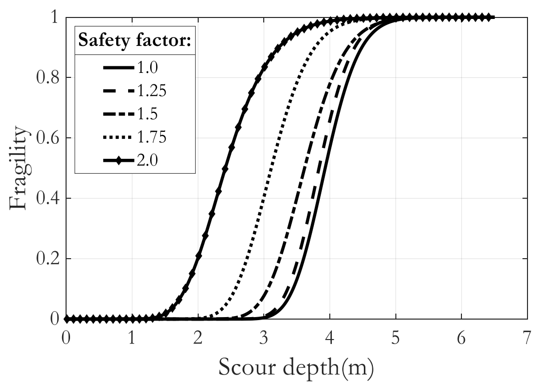

Figure 16. Scour fragility curve.

Table 2. Median and log-standard deviation.

Safety Factor (SF)	Median (m)	Log-Std. (m)
1.00	3.93	0.05
1.25	3.84	0.05
1.50	3.62	0.05
1.75	3.12	0.05
2.00	2.43	0.05

The log-normal standard deviation is equal to 0.05 because, for each SD level, the analysis was carried out by considering only the load variability.

4.7. Scour Risk Assessment

Scour risk was evaluated by integrating the product of scour hazard (SD probability) and scour fragility as given in Equation (3). The scour hazard denoted by $f_{SD}(x)$ was found in Figure 12. It presents the probability density of SD. The fragility denoted by $F_k(x)$

was found in Figure 16 according to SF. SF of 1.0 is the most critical case. Multiplying the scour hazard with the fragility and then integrating them over possible scour depth results in scour risk. Scour risk is expressed as probability of failure, P_f. For convenience, the probability of failure is converted into a reliability index as follows.

$$\beta = -\Phi^{-1}\left(P_f\right) \tag{14}$$

Reliability indices are listed in Table 3 and plotted in Figure 17. The scour risk was 1.919×10^{-7}~0.718 and the reliability index was 5.708~0.578, corresponding to the SF from 1.0 to 2.0. The level of target reliability index (β_t) can be referred from some design standards. DNV GL [29] proposes target failure probability of 10^{-4}, corresponding to β_t of 3.719, while IEC 61400-1 [30] proposes β_t of 3.3. Since the DNV guideline is for offshore wind turbine design, the reliability index was set higher than the IEC standard for onshore wind turbines. Furthermore, compared with the design standards, the reliability index evaluated for the PSB in Gunsan test bed seems higher than those standards if SF is below 1.5.

Table 3. Scour risk and reliability index.

SF	Sour Risk	Reliability Index
1.00	1.919×10^{-7}	5.078
1.25	6.178×10^{-7}	4.850
1.50	6.560×10^{-4}	3.213
1.75	0.058	1.570
2.00	0.718	0.578

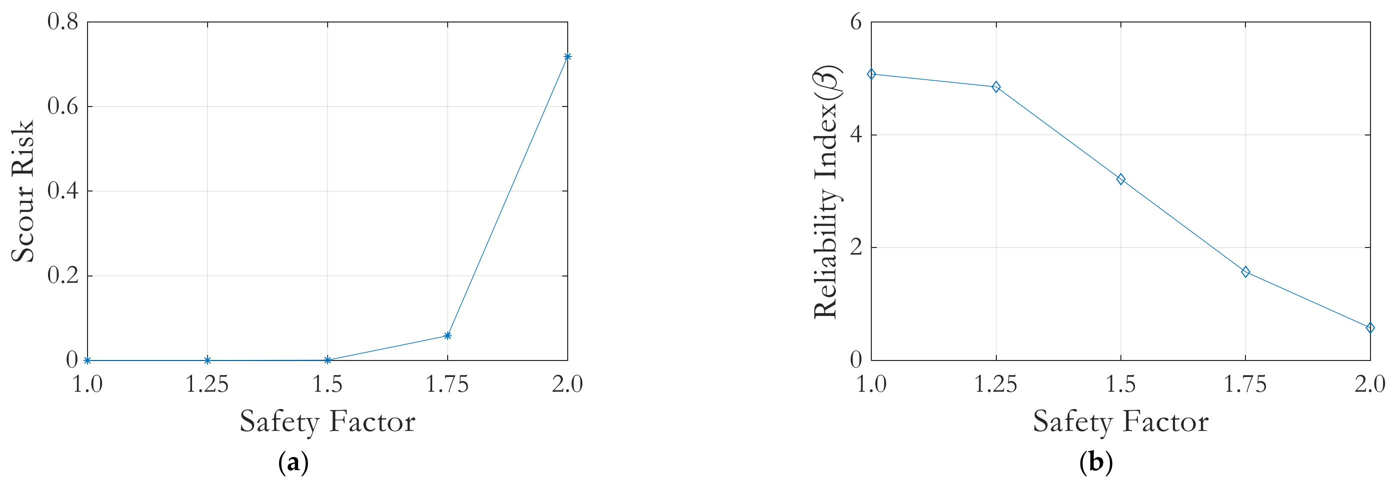

Figure 17. Result of scour risk and reliability index: (**a**) scour risk; (**b**) reliability index.

5. Conclusions

In this study, a scour risk assessment procedure was proposed. Scour hazard was calculated by giving variability to the variables of the empirical formula and was expressed as the probability of the scouring depth. Scour fragility was calculated as the probability that the response of the structure to the environmental load would exceed the limit state. Scour risk was obtained by integrating the product of the scour probability and the fragility for all possible scour depths. The scour risk assessment procedure was applied to PSB supporting 5.5 MW OWT installed on the Gunsan coast in Korea. From the numerical analysis, the reliability index was 4.85 if SF of 1.25 is applied. This level of reliability can be accepted enough when some OWT design standards are used.

Author Contributions: Conceptualization, Y.-J.K. and D.-H.K.; methodology, Y.-J.K. and D.-H.K.; software, Y.-J.K.; validation, D.-H.K.; formal analysis, Y.-J.K.; data curation, Y.-J.K. and D.-V.N.; writing—original draft preparation, Y.-J.K. and D.-V.N.; writing—review and editing, D.-H.K.; supervision, J.-H.L. and D.-H.K. All authors have read and agreed to the published version of the manuscript.

Funding: This research was supported by Basic Science Research Program through the National Research Foundation of Korea (NRF) funded by the Ministry of Education (No. 2020R1F1A1076884).

Institutional Review Board Statement: Not applicable.

Informed Consent Statement: Not applicable.

Data Availability Statement: Not applicable.

Conflicts of Interest: The authors declare no conflict of interest.

References

1. Oh, M.H.; Kwon, O.S.; Kim, K.S.; Jang, I.S. Economic Feasibility of Bucket Foundation for Offshore Wind Farm. *J. Korea Acad.-Ind. Coop. Soc.* **2012**, *13*, 1908–1914. [CrossRef]
2. Latini, C.; Zania, V. Dynamic lateral response of suction caissons. *Soil Dyn. Earthq. Eng.* **2017**, *100*, 59–71. [CrossRef]
3. Achmus, M.; Akdag, C.; Thieken, K. Load-bearing behavior of suction bucket foundations in sand. *Appl. Ocean Res.* **2013**, *43*, 157–165. [CrossRef]
4. Ding, H.; Liu, Y.; Zhang, P.; Le, C. Model tests on the bearing capacity of wide-shallow composite bucket foundations for offshore wind turbines in clay. *Ocean Eng.* **2015**, *103*, 114–122. [CrossRef]
5. Thieken, K.; Achmus, M.; Schröder, C. On the behavior of suction buckets in sand under tensile loads. *Comput. Geotech.* **2014**, *60*, 88–100. [CrossRef]
6. Ngo, D.-V.; Kim, Y.-J.; Kim, D.-H. Seismic Fragility Assessment of a Novel Suction Bucket Foundation for Offshore Wind Turbine under Scour Condition. *Energies* **2022**, *15*, 499. [CrossRef]
7. Yang, Q.; Yu, P.; Liu, Y.; Liu, H.; Zhang, P.; Wang, Q. Scour characteristics of an offshore umbrella suction anchor foundation under the combined actions of waves and currents. *Ocean Eng.* **2020**, *202*, 106701. [CrossRef]
8. Yang, T.; Qi, M.; Wang, X.; Li, J. Experimental study of scour around pile groups in steady flows. *Ocean Eng.* **2020**, *195*, 106651. [CrossRef]
9. Yu, T.; Zhang, Y.; Zhang, S.; Shi, Z.; Chen, X.; Xu, Y.; Tang, Y. Experimental study on scour around a composite bucket foundation due to waves and current. *Ocean Eng.* **2019**, *189*, 106302. [CrossRef]
10. Hu, R.; Wang, X.; Liu, H.; Lu, Y. Experimental Study of Local Scour around Tripod Foundation in Combined Collinear Waves-Current Conditions. *J. Mar. Sci. Eng.* **2021**, *9*, 1373. [CrossRef]
11. Hu, R.; Liu, H.; Leng, H.; Yu, P.; Wang, X. Scour Characteristics and Equilibrium Scour Depth Prediction around Umbrella Suction Anchor Foundation under Random Waves. *J. Mar. Sci. Eng.* **2021**, *9*, 886. [CrossRef]
12. Esteban, M.D.; Lopez-Gutierrez, J.S.; Negro, V.; Sanz, L. Riprap scour protection for monopiles in offshore wind farms. *J. Mar. Sci. Eng.* **2019**, *7*, 440. [CrossRef]
13. Lee, J.H.; Han, T.H.; Kim, S.B.; Yoon, G.L. Dynamic Instability Analysis of Wind Turbines with Mono Pile Foundation Considering Foundation Scour. In Proceedings of the Korean Society of Civil Engineers Conference 2013, Jeongseon-gun, Korea, 23–25 October 2013; pp. 892–896.
14. Ma, H.; Yang, J.; Chen, L. Effect of scour on the structural response of an offshore wind turbine supported on a tripod foundation. *Appl. Ocean Res.* **2018**, *73*, 179–189. [CrossRef]
15. Yanmaz, A.M.; Calamak, M. Evaluation of scour risk at foundations of river bridges. *Tek. Dergi/Tech. J. Turk. Chamb. Civ. Eng* **2016**, *27*, 7533–7549.
16. Khalid, M.; Muzzammil, M.; Alam, J. Reliability analysis of local scour at bridge pier in clay-sand mixed sediments. *Aquademia* **2018**, *2*, 1. [CrossRef]
17. Homaei, F.; Najafzadeh, M. A reliability-based probabilistic evaluation of the wave-induced scour depth around marine structure piles. *Ocean Eng.* **2020**, *196*, 106818. [CrossRef]
18. Kim, Y.J.; Lee, D.Y.; Kim, D.H. Risk Assessment of Offshore Wind Turbine Support Structures Considering Scouring. *J. Korean Soc. Coast. Ocean Eng.* **2020**, *32*, 524–530. [CrossRef]
19. Sumer, B.M.; Fredsøe, J. *The Mechanics of Scour in the Marine Environment*; World Scientific: Singapore, 2002. [CrossRef]
20. Shinozuka, M.; Hwang, H.; Reich, M. Reliability Assessment of Reinforced Concrete Containment Structures. *J. Nucl. Eng. Des.* **1984**, *80*, 247–267. [CrossRef]
21. *Bladed Multibody Dynamics User Manual (Ver. 4.4)*; Garrad Hassan & Partners Ltd.: Bristol, UK, 2013.
22. Abaqus, in Dassault Systemes Simulia Corporation. 2020. Available online: https://abaqus-docs.mit.edu/2017/English/SIMACAEEXCRefMap/simaexc-c-docproc.htm (accessed on 3 March 2022).
23. Papadrakakis, M.; Sapountzakis, E.J. *Matrix Methods for Advanced Structural Analysis*, 1st ed.; Elsevier: Amsterdam, The Netherlands, 2018. [CrossRef]

24. Morison, J.R.; Johnson, J.W.; Schaaf, S.A. The force exerted by surface waves on piles. *J. Pet. Technol.* **1950**, *2*, 149–154. [CrossRef]
25. *Report on the Estimation of Deep Sea Design Wave in All Seas II*; Korea Ocean Research & Development Institute: Busan, Korea, 2005.
26. Goda, Y. Revisiting Wilson's formulas for simplified wind wave prediction. *J. Waterw. Port Coast. Ocean Eng.* **2003**, *129*, 93–95. [CrossRef]
27. Available online: http://www.khoa.go.kr/oceangrid/gis/category/observe/observeSearch.do?type=TIDALCURRENT (accessed on 31 December 2019).
28. Bang, S.; Cho, Y. Use of Suction Piles for Mooring of Mobile Offshore Bases. 2001. Available online: https://apps.dtic.mil/sti/pdfs/ADA372819.pdf (accessed on 19 January 2022).
29. Det Norske Veritas. *Design of Offshore Wind Turbine Structures*; Offshore Standard DNV-OS-J101; Det Norske Veritas: Høvik, Norway, 2007.
30. *Wind Turbines Part I: Design Requirements*, 3rd ed.; International Standards IEC 61400-1; International Electrotechnical Commission: Geneva, Switzerland, 2005.